

# Influences of wide binaries on the structures of planetary nebulae

Noam Soker<sup>★</sup>

*Mathematics-Physics, Oranim-University of Haifa, Tivon 36006, Israel*

Accepted 1994 May 10. Received 1994 May 10; in original form 1994 April 7

## ABSTRACT

We examine the influences of the orbital motion of wide binary progenitors on the structures of the descendent planetary nebulae (PNe). We focus on orbital separations in the range  $a \approx 30$  au to a few  $\times 10^3$  au. When the orbital period is much shorter than the mass-loss episode, the effects are of second order in the ratio of orbital to wind velocity, and are therefore small. Very wide binaries with orbital periods comparable to, or longer than, the mass-loss episodes will cause deviations from axisymmetry. At late times the density enhancement in the equatorial plane may resemble the structure of PNe moving through the ISM, or changes in the wind properties. These structural features may indicate the existence of wide binary systems in the cores of planetary nebulae possessing the features.

The results of this paper may be applied to circumstellar matter around more massive stars, such as progenitors of supernovae (SNe), by rescaling the physical properties of the binary orbits and wind velocities.

**Key words:** binaries: general – circumstellar matter – stars: mass-loss – planetary nebulae: general.

## 1 INTRODUCTION

The argument for binary system mechanisms as the cause of axisymmetrical PNe is made on observational (Livio 1982; Bond & Livio 1990), statistical (de Kool 1990; Yungelson, Tutukov & Livio 1993) and theoretical (Webbink 1979; Morris 1987, 1990; Livio & Soker 1988; Soker & Livio 1989; Soker 1990, 1992a, 1994; Livio 1994a,b) grounds. All the theoretical works deal with binary companions that interact directly with the AGB progenitors' envelopes, or interrupt a substantial fraction of the progenitors' winds. If the orbital separation between the progenitor and the secondary is large ( $a \gtrsim 20$  au), however, the secondary will never come into contact with the AGB star's envelope, no Roche lobe overflow will take place, and the secondary will interrupt  $\lesssim 1$  per cent of the progenitor's wind. According to the statistical study of Yungelson et al. (1993), most binary systems of PNe progenitors have this large separation.

As was pointed out by Soker (1993), if the secondary's mass is of the order of the progenitor's mass, then, even if the secondary does not come into contact with the primary, it can still influence the primary's loss in three ways. First, the secondary can tidally speed up the rotation of the AGB envelope. The time-scale for this to occur increases rapidly with orbital separation (Livio & Soker 1983),  $\tau \propto (a/R_1)^8$ , and

thus it is significant only for  $M_2 \gtrsim M_1$  and  $a \lesssim 15$  au, where  $R_1$  is the primary's radius, and  $M_1$  and  $M_2$  are the primary and secondary masses, respectively. The primary is an AGB star, with a typical mass of  $\approx 1 M_\odot$ . In a newly proposed tidal mechanism (Tassoul 1987; Tassoul & Tassoul 1992), the spiralling-in time for a typical AGB star (Soker 1994) is

$$\tau_{\text{dec}} \approx 5 \times 10^5 (a/5R_1)^{49/8} \text{ yr.} \quad (1.1)$$

For  $R_1 = 2$  au, we find that, even with this more efficient mechanism, tidal spin-up will be significant only for  $a \lesssim 30$  au.

Secondly, for  $M_2 \sim M_1$  and  $a \lesssim 50$  au, the orbital motion of the AGB star around the centre of mass is a few  $\times 0.1$  times the escape velocity from the surface of the AGB star. The orbital motion is expected to influence the temporary geometry of the mass loss. In this paper we study this effect in some detail, including much larger orbital separation. The equations that describe the influence of the orbital motion on the mass-loss geometry are written in Section 2.

Thirdly, according to Soker (1993), for large separation and for  $M_2 \sim M_1$ , the primary will rotate around the symmetry axis of the nebula. For  $a \gtrsim 100$  au  $= 1.5 \times 10^{15}$  cm, the orbital period is  $\gtrsim 1000(a/100 \text{ au})^{3/2}$  yr. This is a substantial fraction of the duration time of the superwind at the end of the AGB, and it is longer than a typical formation time of the jets that, presumably (Soker 1992b), form the ansae – the two bright knots found along the symmetry axis of many elliptical PNe. In 500 years the primary will be displaced by

<sup>★</sup> E-mail: soker@phys4.technion.ac.il

$\sim a \approx 10^{15}$  cm. This can introduce some non-axisymmetrical features. For example, if the jets that form the ansae do not expand exactly along the symmetry axis, they can be bent by the superwind material (Soker 1992b).

Tout & Eggleton (1988) postulate that, by means of tidal torque, the companion enhances the mass-loss rate by a factor of

$$1 + 0.01(R_1/0.1R_L)^6, \quad (1.2)$$

where  $R_L$  is the radius of the Roche lobe around the primary. It is likely that the companion will cause a higher mass-loss rate in the equatorial plane. By taking  $R_1 = 2$  au, and a secondary with less than half the primary mass, we see that this effect will be significant only for  $a \lesssim 30$  au.

The secondary accretes mass also from the primary wind. The accretion radius is  $R_a \approx 2GM_2/v_w'^2$ , where  $v_w'$  is the wind velocity measured in the primary's rest frame. From now on we denote by " quantities that are measured in the primary's rest frame, while quantities without " are measured in the centre-of-mass rest frame. The fraction of the wind mass that is intercepted by the secondary is

$$\begin{aligned} \frac{\dot{M}_2}{|\dot{M}_1|} &= \frac{\pi R_a^2}{4\pi a^2} \\ &= 10^{-5} \left( \frac{M_2}{0.2 M_\odot} \right)^2 \left( \frac{v_w'}{15 \text{ km s}^{-1}} \right)^{-4} \left( \frac{a}{200 \text{ au}} \right)^{-2}. \end{aligned} \quad (1.3)$$

The secondary accretes from the equatorial plane, where the accreted fraction is

$$\begin{aligned} \frac{\dot{M}_2}{|\dot{M}_1|_{\text{eq}}} &= \frac{2R_a}{2\pi a} \\ &= 2.5 \times 10^{-3} \frac{M_2}{0.2 M_\odot} \left( \frac{v_w'}{15 \text{ km s}^{-1}} \right)^{-2} \left( \frac{a}{200 \text{ au}} \right)^{-1}. \end{aligned} \quad (1.4)$$

If the secondary is a main-sequence star which itself has a wind, it may not accrete at all, while, if it is a white dwarf, the above accretion rate can cause cataclysmic events. The above discussion shows that there are several processes and effects in binary systems with orbital separation in the range  $a \approx 10$ –30 au which call for further study.

In the above discussion and the rest of the paper, we scale the binary physical parameters according to the statistical results of Yungelson et al. (1993). Thus the secondary is assumed to be a low-mass main-sequence star, although by taking larger masses the results are applicable to white dwarfs as well. The orbital period is given by

$$T = 2830 \left( \frac{M_1 + M_2}{1 M_\odot} \right)^{-1/2} \left( \frac{a}{200 \text{ au}} \right)^{3/2} \text{ yr}. \quad (1.5)$$

In this paper we concentrate on the orbital separations in the range  $a \approx 30$ –2000 au, which corresponds to the orbital period range  $T \approx 150$ – $10^5$  yr. According to the distribution of solar-type field stars given by Duquennoy & Mayor (1991), about one-third of all binary systems of solar-type stars are in this range, and the statistical results of Yungelson et al. (1993) show that most wide binary nuclei of PNe are in this range as well. The orbital velocity of the primary is given

by

$$v_r = 2.1 \frac{M_2}{M_\odot} \left( \frac{M_1 + M_2}{1 M_\odot} \right)^{-1/2} \left( \frac{a}{200 \text{ au}} \right)^{-1/2} \text{ km s}^{-1}. \quad (1.6)$$

The average expansion velocity of PNe is  $15 \text{ km s}^{-1}$  (Olofsson 1993), so that, in our range of interest, the typical ratio of the orbital velocity to the wind velocity,  $\beta' \equiv v_r/v_w'$ , is in the range  $\beta' \approx 0.01$ –0.1. For closer and more massive secondaries,  $\beta'$  can be as high as 0.3. In Section 3 we solve the equations that describe the mass-loss geometry under the influence of the orbital velocity, by expanding the solution in the small parameter  $\beta'$ .

If a mass-loss episode (i.e. a mass-loss period during which the mass-loss rate, velocity and geometry change only slightly) lasts much longer than the orbital period, then we can average the influence of the orbital motion over many orbits. We neglect the interaction between segments of the wind that have different velocities due to the orbital motion, and find that the influence on the descendant PN structure is proportional to  $\beta'^2$ , and is therefore small (Section 3). If, on the other hand, a mass-loss episode lasts for a fraction of an orbital period, then the axisymmetry is broken. Prominent effects will exist if two successive mass-loss episodes occur at different orbital segments, thus having velocity shifts in different directions. Such a process was proposed to have occurred in the formation of the PN NGC 3242 (Soker, Zucker & Balick 1992). In Section 4 we examine the structure in the equatorial plane of very long-period binaries. We summarize in Section 5.

## 2 THE EQUATIONS

As in the previous section, we denote by " quantities that are measured in the primary's rest frame, while quantities without " are measured in the centre-of-mass rest frame. We use the following notation.  $z'$  is the symmetry axis in the primary rest frame, which, together with  $x'$  and  $y'$ , forms a Cartesian coordinate system.  $\theta'$  is the angle from the positive  $z'$  axis, and  $\phi'$  is the longitude measured from the positive  $x'$  axis. The orbital plane coincides with the primary's equatorial plane. The Cartesian coordinate system in the centre-of-mass rest frame is  $(x, y, z)$ , with the origin at the centre of mass, and where the  $x$ ,  $y$  and  $z$  axes are parallel to the  $x'$ ,  $y'$ , and  $z'$  axes, respectively. The spherical coordinate  $\theta$  is the angle from the  $z$  axis and  $\phi$  is the angle in the equatorial plane, measured from the positive  $x$  axis. We denote by  $a$  the angle between the primary position and the positive  $x$  axis. The geometry is illustrated in Fig. 1. In principle, the axisymmetric mass-loss rate and wind velocity  $v_w'(\theta')$  in the primary's rest frame can be functions of  $\theta'$  and the time. For the purpose of this paper, however, it is adequate to take the wind velocity to be constant. The wind velocity in the centre-of-mass rest frame  $v_w(\theta, \phi)$  is a function of both  $\theta$  and  $\phi$ . We denote by  $v_r$  the magnitude of the orbital velocity of the primary, and define  $\beta \equiv v_r/v_w$ .

The wind velocity components in the rest frame of the mass-losing star are

$$\begin{aligned} v_{x'} &= v_w' \sin \theta' \cos \phi', & v_{y'} &= v_w' \sin \theta' \sin \phi', \\ v_{z'} &= v_w' \cos \theta', \end{aligned} \quad (2.1)$$

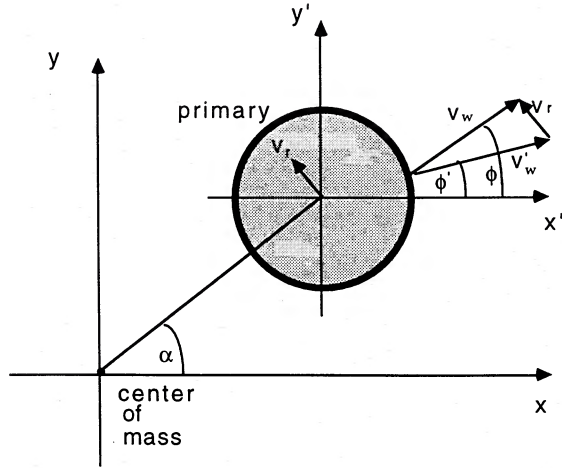


**Figure 1.** The geometry of the binary system in the equatorial plane. The  $z$  and  $z'$  axes are perpendicular to the equatorial plane.  $v_r$  is the primary's orbital velocity and  $v_w$  is the wind velocity in the primary's rest frame.

while the wind velocity components in the centre-of-mass rest frame are

$$v_x = v'_x - v_r \sin \alpha, \quad v_y = v'_y + v_r \cos \alpha, \quad v_z = v'_z. \quad (2.2)$$

To obtain the expression for  $\beta(\theta, \phi) = v_r/v_w(\theta, \phi)$ , we write the component of the wind velocity in the left-hand side of equation (2.2) in a spherical coordinate system, and use the equality  $\beta'^2 = v_r^2/[(v'_x)^2 + (v'_y)^2 + (v'_z)^2]$ . We obtain the following quadratic equation for  $\beta(\theta, \phi)$  (for a constant  $\beta'$ ):

$$\beta^2(1 - \beta'^2) + \beta\beta'^2 2 \sin \theta \sin(\phi - \alpha) - \beta'^2 = 0. \quad (2.3)$$

The wind velocity is  $v_w(\theta, \phi) = v_r/\beta(\theta, \phi)$ .

The direction  $(\theta, \phi)$  of a mass element that leaves the primary in the direction  $(\theta', \phi')$  is given by

$$\begin{aligned} \tan \theta &= \frac{(v_x^2 + v_y^2)^{1/2}}{v_z} \\ &= \frac{1}{\cos \theta'} [\sin^2 \theta' + 2\beta' \sin \theta' \sin(\phi' - \alpha) + \beta'^2]^{1/2}, \\ \tan \phi &= \frac{v_y}{v_x} = \frac{\sin \theta' \sin \phi' + \beta' \cos \alpha}{\sin \theta' \cos \phi' - \beta' \sin \alpha}. \end{aligned} \quad (2.4)$$

Equations (2.3) and (2.4) give the velocity and direction of the wind relative to the centre of mass.

We next calculate the mass loss per unit solid angle. We examine a mass element leaving the star in a solid angle  $d\theta' \sin \theta' d\phi'$ . The vectors  $d\theta' \hat{\theta}'$  and  $\sin \theta' d\phi' \hat{\phi}'$  are projected into

$$d\theta' \hat{\theta}' \rightarrow d\theta' \left( \frac{\partial \theta}{\partial \theta'} \hat{\theta} + \frac{\partial \phi}{\partial \theta'} \sin \theta \hat{\phi} \right),$$

and

$$\sin \theta' d\phi' \hat{\phi}' \rightarrow d\phi' \left( \frac{\partial \theta}{\partial \phi'} \hat{\theta} + \frac{\partial \phi}{\partial \phi'} \sin \theta \hat{\phi} \right). \quad (2.5)$$

The corresponding solid angle projection is obtained by a vector multiplication of the two projected vectors given in equation (2.5):

$$\begin{aligned} d\theta' \sin \theta' d\phi' &\rightarrow d\theta' \sin \theta' d\phi' S(\theta', \phi') \\ &= d\theta' d\phi' \left| \frac{\partial \theta}{\partial \theta'} \frac{\partial \phi}{\partial \phi'} - \frac{\partial \phi}{\partial \theta'} \frac{\partial \theta}{\partial \phi'} \right| \sin \theta, \end{aligned} \quad (2.6)$$

where the equality defines the function  $S$ . Upon substituting  $\theta$  and  $\phi$  from equations (2.4) into (2.6), we find the expression for  $S$ :

$$S(\theta', \phi') = \frac{1 + \beta' \sin \theta' \sin(\phi' - \alpha)}{[1 + 2\beta' \sin \theta' \sin(\phi' - \alpha) + \beta'^2]^{3/2}}. \quad (2.7)$$

We denote by  $\Delta M'(\theta')$  the mass per unit solid angle leaving the primary. The corresponding mass per unit solid angle in the centre-of-mass rest frame is  $\Delta M(\theta, \phi) = \Delta M'(\theta')/S(\theta', \phi')$ . Equations (2.3), (2.4) and (2.7) contain the necessary information on the emerging wind, as measured in the centre-of-mass rest frame.

### 3 SOLUTION BY SERIES EXPANSIONS

To obtain manageable expressions for the wind properties in the centre-of-mass rest frame, we expand the variables in the small parameter  $\beta'$ . The orbital separations we study have  $\beta' < 0.3$ , with typical values of  $\beta' \sim 0.1$ . We therefore expand up to the third order in  $\beta'$ . The solution of equation (2.3) for  $\beta$  reads

$$\frac{\beta(\theta, \phi)}{\beta'} = 1 - \beta' \Psi + \frac{1}{2} \beta'^2 (1 + \Psi^2) - \beta'^3 \Psi + O(\beta'^4), \quad (3.1)$$

where we define the function

$$\Psi(\theta, \phi) \equiv \sin \theta \sin(\phi - \alpha). \quad (3.2)$$

Expansion of equation (2.7) yields

$$\begin{aligned} S^{-1}(\theta, \phi) &= 1 + 2\beta' \sin \theta' \sin(\phi' - \alpha) \\ &\quad + \frac{1}{2} \beta'^2 [3 - \sin^2 \theta' \sin^2(\phi' - \alpha)] + O(\beta'^4), \end{aligned} \quad (3.3)$$

where the third order's coefficient vanishes. Using the inverse equations to equations (2.4), with  $\beta' \rightarrow -\beta$ , we find

$$\sin \theta' \sin(\phi' - \alpha) = \Psi + \beta(\Psi^2 - 1) + \frac{3}{2} \beta^2 (\Psi^3 - \Psi) + O(\beta'^3). \quad (3.4)$$

Substitution of (3.1) into (3.4) and then into (3.3) gives, up to the third order in  $\beta'$ ,

$$S^{-1}(\theta, \phi) = 1 + 2\beta' \Psi + \frac{1}{2} \beta'^2 (3\Psi^2 - 1) + \frac{3}{2} \beta'^3 (\Psi^3 - \Psi). \quad (3.5)$$

If the mass-loss episode continues for a time much longer than the orbital period, we can average the mass loss per unit solid angle over many orbits, to obtain an axisymmetrical wind geometry. For simplicity we take the mass-loss rate per unit solid angle from the primary to be constant and use the expansion (3.5) for  $S^{-1}$ . We find, for the total mass loss per unit solid angle,

$$\langle \Delta M(\theta) \rangle = \frac{1}{2\pi} \int_0^{2\pi} \frac{\Delta M'}{S(\theta, \phi)} d\alpha = \Delta M' \left[ 1 + \beta'^2 \left( \frac{3}{4} \sin^2 \theta - \frac{1}{2} \right) \right]. \quad (3.6)$$

Integration of  $\Delta M$  from  $\theta=0$  to  $\pi$  gives the total mass in the wind  $2\pi \int \langle \Delta M(\theta) \rangle \sin \theta d\theta = 4\pi \Delta M'$ , as it should be from mass conservation.

To find the average wind velocity, we first write the expansion of the velocity by using equation (3.1) for  $\beta$ . This gives

$$v_w(\theta, \phi) = \frac{v_r}{\beta} = v'_w \left[ 1 + \beta' \Psi + \frac{1}{2} \beta'^2 (\Psi^2 - 1) + O(\beta'^4) \right]. \quad (3.7)$$

Using this for the wind velocity and equation (3.5) for  $S^{-1}$  in the expression  $\Delta M = \Delta M'/S$ , we find the average wind velocity as a function of  $\theta$ :

$$\begin{aligned} \langle v_w(\theta) \rangle &= \left[ \int_0^{2\pi} \Delta M(\theta, \phi) d\alpha \right]^{-1} \int_0^{2\pi} \Delta M(\theta, \phi) v_w(\theta, \phi) d\alpha \\ &= v'_w \left[ 1 + \beta'^2 \left( \frac{5}{4} \sin^2 \theta - \frac{1}{2} \right) \right]. \end{aligned} \quad (3.8)$$

We remember that the above equation was derived under the assumption of uniform mass loss  $\Delta M'$ , and constant wind velocity  $v'_w$ , from the surface of the primary.

From equation (3.6) for the mass-loss geometry and equation (3.8) for the average velocity, we see that the influence of the orbital motion in close binaries is only of second order in the orbital velocity. The main shells of PNe are formed from mass-loss episodes which last  $\lesssim 10\,000$  yr. From equation (1.5), we see that to average over orbital periods is reasonable for orbital separations of  $a \lesssim 200$  au. Taking  $M_2 \lesssim 1 M_\odot$  in equation (1.6) for the orbital velocity  $v_r$ , and with wind velocity  $v'_w \approx 10 \text{ km s}^{-1}$ , we find that  $\beta' \equiv v_r/v'_w \lesssim 0.2$ . The differences between the equatorial plane and the poles will be less than 5 per cent. More typical parameters have shorter orbital periods, with  $a \sim 50$  au, secondary masses of  $M_2 \lesssim 0.4 M_\odot$ , and a wind velocity of  $15 \text{ km s}^{-1}$ . These parameters yield  $\beta < 0.1$ , which results in equator-poles differences of less than 1 per cent. Such low deviations are almost impossible to detect, since most PNe possess much larger deviations from sphericity, which are caused by other factors. The cases where such effects may be detected are in large spherical haloes, similar to the halo of NGC 6826. The halo of NGC 6826 is large and seems to expand slowly (Plait & Soker 1990). The mass-loss episode that formed this spherical halo occurred over more than  $10\,000$  yr. Small axisymmetrical deviations from sphericity may result from wide binaries. But, here again, even if we find a very small axisymmetric deviation from sphericity in the halo of NGC 6826, it will be hard to determine that this deviation was not caused by the same process that caused the inner region to be axisymmetric, rather than by a wide binary companion.

On the other hand, wide binaries with orbital periods comparable to, or longer than, the mass-loss episodes will cause deviations from axisymmetry as well. As shown by equations (3.5) and (3.7), the difference between the two sides in the equatorial plane is of the order of  $2\beta'$ . From equations (1.5) and (1.6), for the orbital period and velocity, we find

$$\begin{aligned} 2\beta' &= 0.037 \left( \frac{M_2}{0.2 M_\odot} \right) \left( \frac{M_1 + M_2}{1 M_\odot} \right)^{-2/3} \left( \frac{T}{1 \times 10^4 \text{ yr}} \right)^{-1/3} \\ &\quad \times \left( \frac{v'_w}{15 \text{ km s}^{-1}} \right)^{-1}. \end{aligned} \quad (3.9)$$

Differences in the velocity or in the distance from the central star of a few per cent, between two sides in the equatorial plane of shells in typical PNe, can be detected. Soker et al. (1992) find a deviation of  $\lesssim 10$  per cent between the two equatorial sides of NGC 3242, and estimate that the binary period is  $\sim 4000$  yr. For a wind velocity of  $10 \text{ km s}^{-1}$ , they show that a  $0.6 M_\odot$  companion at 250 au can explain the deviation. Equation (3.9) demonstrates that, with an orbital period of 4000 yr, a companion of  $\sim 0.3 M_\odot$  can, indeed, cause the deviation from axisymmetry of NGC 3242. To understand better the effect of wide binaries, we turn next to an illustration of the structure in the equatorial plane.

#### 4 THE STRUCTURE OF THE NEBULA IN THE EQUATORIAL PLANE

We examine a mass-loss episode that started at a time  $t_p$  before present. We take the wind to be composed of freely streaming mass elements, which is equivalent to assuming a flow with a high Mach number. The wind velocity in each direction will change according to the direction of the primary orbital motion (see equation 3.7). Parcels of gas leaving the primary at high velocities will catch up with parcels moving slower in the same direction, and interact with them hydrodynamically. We neglect this interaction. We further decompose the wind into pulses, with constant time intervals between consecutive pulses, and with spherically symmetric mass loss from the primary surface. We set the time to be  $t=0$  at the beginning of the mass-loss process, so that presently  $t=t_p$ . We terminate the mass-loss process after a period of 3000 yr. We take the coordinate system in the equatorial plane  $(x, y)$ , such that the positive  $x$  axis coincides with the primary location at  $t=0$ , and the origin is at the centre of mass.

The primary position at time  $t$  is given by

$$x_1(t) = a_1 \cos(2\pi t/T), \quad y_1(t) = a_1 \sin(2\pi t/T), \quad (4.1)$$

where  $T$  is the orbital period and  $a_1 = aM_2/(M_1 + M_2)$  is the distance of the primary from the centre of mass.

Each pulse of mass loss will form a spherical surface, moving at the wind velocity  $v'_w$  relative to the sphere centre. The radius of the sphere is given by

$$R(t) = (t_p - t) v'_w. \quad (4.2)$$

The velocity of the centre of the sphere relative to the centre of mass is equal to the primary velocity at the time it released the pulse:

$$u_x(t) = -v_r \sin(2\pi t/T), \quad u_y(t) = v_r \cos(2\pi t/T). \quad (4.3)$$

Presently the centre of each pulse is at

$$\begin{aligned} x_p(t) &= x_1(t) + (t_p - t) u_x \\ &= a_1 \left[ \cos(2\pi t/T) - 2\pi \frac{(t_p - t)}{T} \sin(2\pi t/T) \right], \\ y_p(t) &= y_1(t) + (t_p - t) u_y \\ &= a_1 \left[ \sin(2\pi t/T) + 2\pi \frac{(t_p - t)}{T} \cos(2\pi t/T) \right], \end{aligned} \quad (4.4)$$

where we have used the relation  $v_r = 2\pi a_1/T$ . The orbital period is related to the orbital separation and the stars' masses by equation (1.5).

In Fig. 2 we draw the intersections of the mass-loss pulse shells with the equatorial plane. The gas density of the real nebula is proportional to the densities of the shells drawn in the figure. The binary parameters and the present time are written in each panel. The primary and secondary masses are  $M_1 = 0.8 M_\odot$  and  $M_2 = 0.2 M_\odot$ , respectively; the time dif-

ference between the first and last pulses is 3000 yr, and the wind velocity is  $10 \text{ km s}^{-1}$ .

Equation (4.4) demonstrates that, when the orbital period  $T$  is comparable to  $2\pi(t_p - t)$ , the effects of the orbital radius and orbital velocity on the shell's position are of the same order. This is illustrated in the upper left panel of Fig. 2, at  $t_p = 4000$  yr. For the inner shell,  $2\pi(t_p - t) \approx 6000$  yr, which is close to the orbital period of 8000 yr. At the time of the last mass-loss pulse, the primary was in the direction of  $\sim 45^\circ$  left

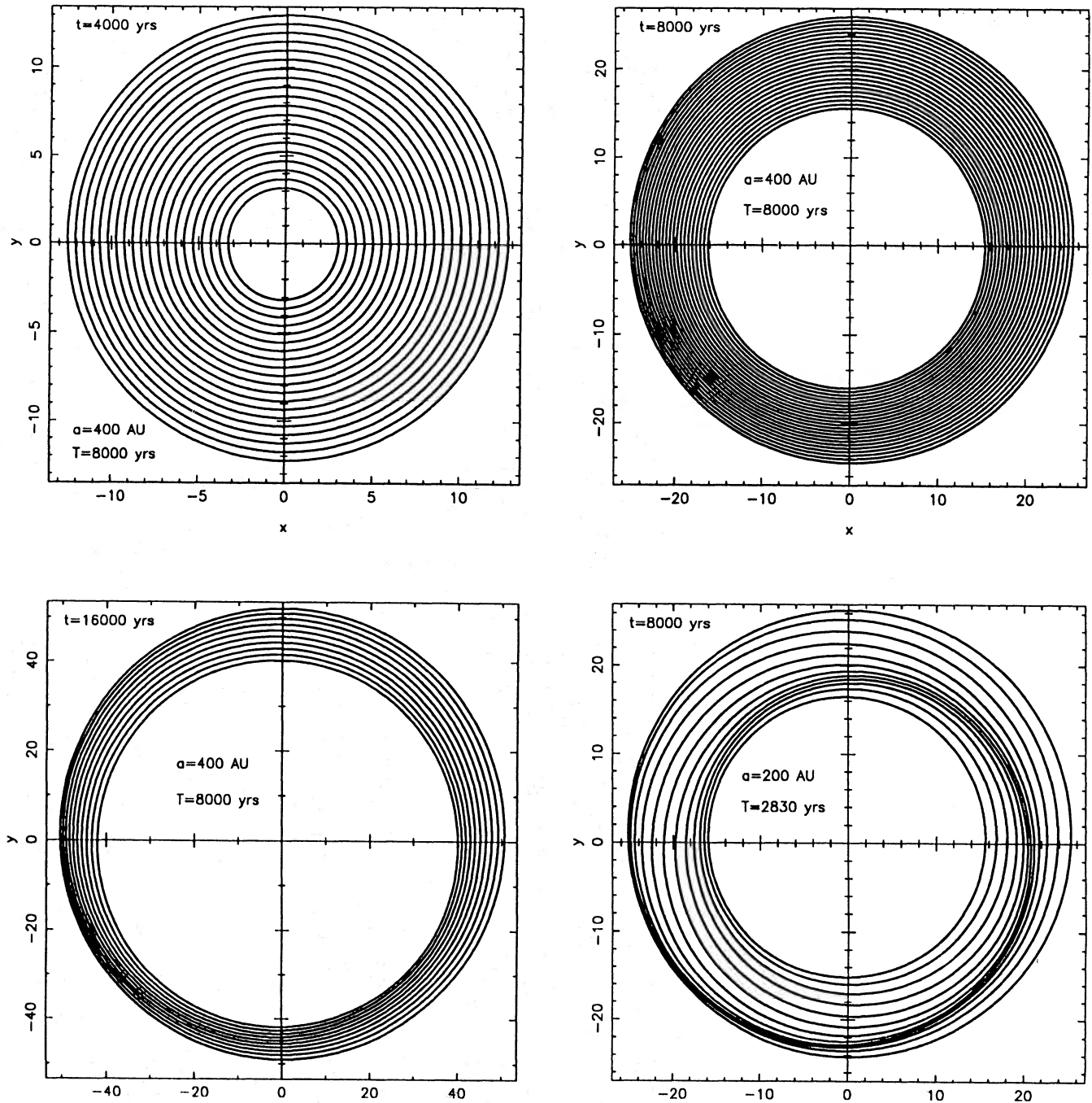


**Figure 2.** The intersections of the mass-loss pulse shells with the equatorial plane, for two binary systems. The units on the axes are  $10^{16}$  cm, and  $a$  and  $T$  are the binary systems' orbital separations and periods, respectively.  $t$  is the time since the first pulse took place, while the last pulse happened 3000 yr after the first pulse.

of the positive  $y$  axis, moving counterclockwise. The effects of the position and velocity of the primary are of the same order, with an opposite contribution along the  $y$  direction and the same contribution along the  $x$  direction. As a result, the inner shell is displaced toward the negative  $x$  direction.

At the first pulse, the primary was at  $80 \text{ au} = 1.2 \times 10^{15} \text{ cm}$  on the positive  $x$  axis, moving in the positive  $y$  direction. The outer shell is displaced mainly in the positive  $y$  direction, but a  $\sim 1$  per cent displacement to the right may also be noticed. We remember that the orbital velocity changes the velocity of the gas, a process which leads to interactions between consecutive mass-loss pulses, and which we do not treat here.

At late times,  $(t_p - t) \gg T/(2\pi)$ , the influence of the primary's location at the time of mass loss may be neglected, and the shape of the PN shell is scaled with the ratio of orbital to wind velocity  $\beta'$ . Therefore the results presented here at late times can be rescaled to other binary parameters. The 3000-yr mass-loss episode is plotted after 8000 yr (upper right panel) and after 16 000 yr (lower left panel). Note that the numbers of shells drawn were chosen in order to present the structure in the best manner, and are not the same in the different panels. In these two panels, the lower left portion of the shell is denser, as a result of the higher velocity of the late pulses in this direction, relative to the early pulses. The mass-loss episode lasted for 37 per cent of the orbital period, which resulted in about the same fraction of the shell having density enhancement. In the lower right panel we draw 12 pulses for an orbital separation of  $a = 200 \text{ au}$ . Here the mass-loss episode duration was about equal to the orbital period, and the spiral density enhancement encircles the shell once. At later times, consecutive pulses cross one another, which means that the gas interacts hydrodynamically with itself. Hence our presentation is meaningless for later times.

When interpreting these images one must remember that, in most cases, the mass loss would not be spherical, and the effects of the wide binaries would add up to larger deviations from sphericity in the mass-loss process itself. In any case, the outer parts of PNe tend to be more spherical, and the structure presented in the lower left panel may be confused with a motion of the nebula through the ISM, or with a change in the mass-loss rate. To distinguish this structure from the above mentioned processes, specific structural features of wide binaries should be used. The density enhancement by the wide binary mechanism, for example, is continuous and has a spiral shape. Thus two separated arcs, such as those of the interacting PN A 34 (Tweedy & Kwitter 1994), may not be explained as the effect of a binary companion.

Let us examine the PN Sp 1, which is known to contain a close binary core (Bond & Livio 1990). Bond & Livio further argue that the orbital plane is almost perpendicular to the line of sight, and that the nebula is more of a ring shape. The nebula of Sp 1 contains a thin bright incomplete rim to the west side. It somewhat resembles the structure of the lower left panel of Fig. 2, but the density enhancement region has an elliptical, rather than a spiral, shape. It is plausible that, due to inclination and hydrodynamical effects, the bright thin shell appears elliptical. A two-dimensional hydrodynamical code is necessary to find whether structures of bright thin incomplete elliptical shells, such as the one in the nebula of Sp 1, can be explained by wide binaries [the main ring-shaped nebula of Sp 1 may be explained by the close binary (Bond & Livio 1990)].

The best way to look for influences of wide binaries is to examine whether some structural features may be attributed to the effects of wide binary systems, when studying and analysing specific nebulae (as Soker et al. 1992 did for NGC 3242).

## 5 SUMMARY

In this paper we examine the influences of the orbital motion of wide binary progenitors on the structures of the descendant PNe. The processes studied are relevant to binaries with orbital separations in the range  $a \approx 30 \text{ au}$  to a few  $\times 10^3 \text{ au}$ . Below this range, other effects, which demand further study, are more influential, while above this range (depending on the secondary mass) the orbital motion is too slow, and the orbital period too long, to cause noticeable structural imprints on the descendent PNe. We write the equations that give the wind geometry and velocity in the centre-of-mass rest frame, by using the parameter  $\beta'$ , which is the ratio of orbital to wind velocity. For the binaries examined here,  $\beta'$  is a small parameter ( $\beta' \lesssim 0.1$ ). The results of this paper may be applied to circumstellar matter around more massive stars, such as progenitors of SNe, by rescaling the physical properties of the binary orbits and wind velocities.

In Section 3 we examine cases where the orbital period is much shorter than the mass-loss episode, and expand the solution in the small parameter  $\beta'$ . We average over many orbital periods to obtain axisymmetrical effects. We find (equations 3.6 and 3.8) that the effects are only of second order in the ratio of orbital to wind velocity  $\beta'$ . Since  $\beta' \lesssim 0.1$ , the influences on the nebular structures are small.

Very wide binaries, for which the orbital period is comparable to or longer than the mass-loss episode, will cause deviations from axisymmetry. At early times both the primary's distance from the centre of mass and its orbital velocity affect the nebular structure (left-upper panel of Fig. 2), while at later times the ratio of orbital to wind velocity is the significant parameter. At late times the density enhancement in the equatorial plane may resemble the structure of PNe moving through the ISM (lower-left panel of Fig. 2), or changes in the wind properties. Some specific features, such as continuous density rim and spiral structure in wide binaries, can be used to distinguish between wide binary effects and other effects.

The effects of wide binaries may be best noticed when changes in the wind properties, such as a transition to a superwind or the formation of jets, exist. The orbital periods of wide binaries, which can be much shorter than the main nebular formation times, can still be longer than the jets' formation time (few  $\times 100 \text{ yr}$ ). The two opposite jets would not expand along the symmetry axis of the nebula, but rather would both decline to the symmetry axis in the same direction. Jets that decline in the same direction are unlikely to be formed by precession, which causes the two opposite jets to expand exactly in opposite directions. Jets, or ansae, that are declined in the same direction relative to the symmetry axis of the main nebula may be seen in the images of NGC 2022, 3242 and 6826 (Balick 1987). Another PN that has a structure that might be explained by the presence of a wide binary system is NGC 7662. The central star of this PN is displaced south-east toward the rim, with bright knots concentrated in the same direction (Balick 1987).

The changes in wind properties and hydrodynamical interactions in the nebulae were not studied here. A two-

dimensional, or even three-dimensional, study of these properties, with direct comparison to observations, is strongly encouraged. This is in addition to the effects of binaries with orbital separations of  $a \approx 10\text{--}30$  au, which call for both more analytical and more numerical research.

#### ACKNOWLEDGMENTS

I thank Orit Ben-Zeev for her careful reading of the manuscript, and Achiam Wiener for his help with the graphics. This work has been supported by the Allon fellowship.

#### REFERENCES

- Balick B., 1987, *AJ*, 94, 671  
 Bond H., Livio M., 1990, *ApJ*, 355, 568  
 de Kool M., 1990, *ApJ*, 358, 189  
 Duquenois A., Mayor M., 1991, *A&A*, 248, 455  
 Livio M., 1982, *A&A*, 105, 37  
 Livio M., 1994a, in Acker A., ed., *Proc. IAU Symp., Planetary Nebulae*. In press  
 Livio M., 1994b, in Clegg R. E. S., ed., *Proc. 34th Herstmonceux Conf., Circumstellar Media in the Late Stages of Stellar Evolution*. Cambridge Univ. Press, Cambridge, in press  
 Livio M., Soker N., 1983, *A&A*, 125, L12  
 Livio M., Soker N., 1988, *ApJ*, 329, 764  
 Morris M., 1987, *PASP*, 99, 1115  
 Morris M., 1990, in Mennessier M. O., Omont A., eds, *From Miras to Planetary Nebulae: Which Path for Stellar Evolution?* Editions Frontières, Gif-sur-Yvette, p. 520  
 Olofsson H., 1993, in Schwarz H. E., ed., *Proc. Second ESO/CTIO Workshop on Mass Loss on the AGB and Beyond*. ESO, Garching bei München, p. 330  
 Plait P., Soker N., 1990, *AJ*, 99, 1883  
 Soker N., 1990, *AJ*, 99, 1869  
 Soker N., 1992a, *ApJ*, 386, 190  
 Soker N., 1992b, *ApJ*, 389, 628  
 Soker N., 1993, in Schwarz H. E., ed., *Proc. Second ESO/CTIO Workshop on Mass Loss on the AGB and Beyond*. ESO, Garching bei München, p. 18  
 Soker N., 1994, *PASP*, 106, 59  
 Soker N., Livio M., 1989, *ApJ*, 339, 268  
 Soker N., Zucker D. B., Balick B., 1992, *AJ*, 104, 2151  
 Tassoul J.-L., 1987, *ApJ*, 322, 856  
 Tassoul J.-L., Tassoul M., 1992, *ApJ*, 395, 259  
 Tout C. A., Eggleton P. P., 1988, *MNRAS*, 231, 823  
 Tweedy R. W., Kwitter K. B., 1994, *AJ*, 108, 188  
 Webbink R. F., 1979, in Bateson F. M., Smak J., Urch I. H., eds, *Proc. IAU Colloq. 46, Changing Trends in Variable Star Research*. Hamilton, New Zealand, p. 102  
 Yungelson L. R., Tutukov A. V., Livio M., 1993, *ApJ*, 418, 794